Journal of Materials Chemistry A

ROYAL SOCIETY OF CHEMISTRY

PAPER

View Article Online
View Journal

Check for updates

Cite this: DOI: 10.1039/d6ta00298f

Superspreading-photoinitiated *in situ* construction of a hydrogel electrolyte enabling high-performance and long-cycling zinc-ion batteries

Jihao Fan,[ab] Linlin Ma,*[ab] Ziqiang Zhao,[ab] Meng Yu,[ab] Yue Wu,[ab] Shengwen Kong,*[ab] Yanglansen Cui*[ab] and Chuangqi Zhao *[ab]

Received 12th January 2026
Accepted 20th February 2026

DOI: 10.1039/d6ta00298f

rsc.li/materials-a

Hydrogel electrolytes have emerged as a research focus for flexible aqueous zinc ion batteries under extreme environments. This prominence arises from the synergistic effect between tunable functional groups within their polymer networks and confined solvent molecules, conferring unique properties including fast ionic conductivity, enhanced mechanical properties, and good flexibility. However, the weak-bonding interface between the Zn anode and hydrogel electrolytes poses a challenge to achieve high electrochemical performance batteries. Herein, we prepared a carboxymethyl cellulose/polyacrylamide hydrogel electrolyte with a well-integrated electrode–electrolyte interface *via* superspreading of a pre-polymerization solution on a superhydrophilic-treated Zn anode surface, combining *in situ* photoinitiated polymerization. With high Zn^{2+} transference number (0.83) of the obtained hydrogel electrolyte, the interfacial Zn^{2+} concentration is largely improved, which effectively suppresses Zn dendrite growth. Consequently, the hydrogel electrolyte endows the Zn//Zn symmetric cell with stable zinc stripping/deposition up to 2400 hours at 0.5 mA cm^{-2} and 0.5 mA h cm^{-2}. The assembled full cell exhibited significantly enhanced cycling stability, with a capacity retention rate as high as 91% after 2000 cycles even at low temperatures of −20 °C. This strategy realizes a robust interface and offers scalability potential, which provides a viable pathway toward the practical application of sustainable zinc-ion batteries.

Introduction

The rapid development of renewable energy and electric vehicles has escalated the demand for large-scale energy storage systems, intensifying the pursuit of high safety, low cost, and environmentally benign battery technologies.[1–3] Among the emerging alternatives, aqueous zinc-ion batteries (AZIBs) have attracted significant attention due to their intrinsic advantages, including the high theoretical capacity of Zn anodes (820 mA h g^{-1}), appropriate redox potential (−0.76 V *vs.* standard hydrogen electrode), and natural abundance of zinc resources.[4] Meanwhile, the stability of zinc-ion batteries is significantly compromised by rampant zinc dendrite growth and water-induced parasitic reactions. These issues lead to unfavorable volume expansion and short-circuiting of zinc anodes, accompanied by the formation of irreversible by-products at the electrolyte–electrode interface. In order to protect Zn anodes from dendrite growth, side reactions and corrosion, it is key to develop an efficient and scalable interfacial engineering strategy.[5,6] Gel polymer electrolytes (GPEs), combining the ionic conductivity of liquids with the mechanical stability of solids, offer a potential solution for modulating Zn deposition behavior and extending battery lifespan.[7,8] The hydrogel network contains abundant polar functional groups (such as –COOH, $–CONH_2$, –OH, *etc.*) that can guide the uniform deposition of Zn^{2+} through coordination effects.[9,10] CMC possesses abundant polar groups (–OH, $–COO^-$) that can replace water molecules in the Zn^{2+} solvation shell, reducing water activity to minimize hydrogen evolution reactions and corrosion.[11,12] Simultaneously, the electrostatic shielding layer or three-dimensional network formed by CMC can homogenize the electric field distribution and guide Zn^{2+} to preferentially deposit along the (002) crystal plane, promoting dense and uniform zinc deposition layers.[13] Additionally, it enhances the electrolyte's ionic conductivity, Zn^{2+} migration number, and interfacial wettability.[14] PAM, with its excellent salt resistance, can stably coexist with high-concentration liquid-phase zinc salts while maintaining structural integrity, addressing the pain point of salt-induced degradation in traditional gel matrices. Its polymer backbone disrupts hydrogen bonds between water molecules, ensuring ionic conductivity across a wide

[a]State Key Laboratory of Bioinspired Interfacial Materials Science, School of Chemistry and Materials Science, University of Science and Technology of China, Hefei 230026, China. E-mail: zhaochuangqi@ustc.edu.cn; yanglansen.cui@ustc.edu.cn; malinlin@mail.ustc.edu.cn; kongsw@ustc.edu.cn

[b]Suzhou Institute for Advanced Research, University of Science and Technology of China, Suzhou, 215123, P.R. China

temperature range. Through strong hydrogen bonding between molecular chains and physical entanglement of chain segments, PAM forms a semi-penetrating network with CMC, significantly compensating for the mechanical strength deficiency of pure PAM hydrogels. Furthermore, the abundant hydrogen bond sites (–$CONH_2$ in PAM and –COOH in CMC) can restructure stable hydrogen bond networks with water molecules, further confining isolated water molecules and suppressing their activity and proton diffusion. This ultimately achieves comprehensive optimization of electrolyte mechanical properties, wide-temperature adaptability, and electrochemical stability, synergistically enhancing the cycle life, rate performance, and extreme environmental adaptability of zinc symmetric and full batteries.[15] Traditional GPEs are fabricated *ex situ* as pre-prepared thin films and sandwiched between electrodes during battery assembly. This poor interfacial bonding results in high interfacial impedance and leads to uneven ion transport flux. Furthermore, when pre-formed GPEs are immersed in Zn^{2+}-containing solutions for activation, the abundant interfacial water molecules exacerbate parasitic reactions.[16,17] *In situ* polymerization of GPEs directly on the electrode surface can overcome these limitations. By infiltrating liquid monomers prior to gelation, this approach enables chemical bonding, creating a densely integrated interface that simultaneously mitigates physical defects and suppresses interfacial free-water activity. The currently reported methods for *in situ* preparation of hydrogel electrolytes include chemical modification and chemical welding of Zn anodes.[18,19] However, these approaches involve complex fabrication processes and present difficulties in achieving large-scale production.[20] Herein, we reported a superspreading combined with a photo-initiated polymerization strategy to fabricate a large-area hydrogel electrolyte *in situ* on the surface of superhydrophilic Zn anodes. This hydrogel electrolyte can form a tight bonding interface with the Zn anode, which facilitates rapid ion transport and minimizes free water content. Thus, the hydrogel electrolyte exhibits an excellent ionic conductivity of 23.6 mS cm^{-1} and superior Zn^{2+} transference number of 0.83. Furthermore, the hydrogel electrolyte enables the Zn//Zn symmetric cell to achieve over 2400 hours of reversible plating/stripping. The Zn//PANi full cell shows a high initial specific capacity of 175 mA h g^{-1} at 0.5 A g^{-1}, retaining 139 mA h g^{-1} specific capacity after 2000 cycles. Note that, even at −20 °C, the full cell maintains an initial specific capacity of 100.4 mA h g^{-1} and maintains 91% of the capacity after 2000 cycles. This approach significantly enhances the stability and cycle life of AZIBs, providing a viable and promising pathway for the development of next-generation AZIBs.

Results and discussion

Preparation and characterization of the SP-CMC-PAM hydrogel electrolyte

Conventionally, a weak bonding solid–solid interface is typically formed between *ex situ* prepared hydrogel electrolytes and a Zn anode. These interfaces progressively degrade during cycling due to parasitic reactions and dendrite growth.[21] During the charging/discharging process of AZIBs, Zn^{2+} is typically desolvated from the electrolyte and deposited onto the Zn anode, initially forming small protrusions (Fig. 1a). The inhomogeneous interface enhances the local electric field, leading to the "tip effect", which further aggravates Zn dendrite growth. Furthermore, Zn's strong reducing nature relative to hydrogen drives reactions with interfacial free water, leading to the hydrogen evolution reaction (HER) and surface corrosion. In contrast, the *in situ* polymerized hydrogel electrolyte reduces the electrochemical activity of free water molecules, effectively suppressing the HER and zinc corrosion. Meanwhile, the polymer porous networks contain abundant carboxyl groups, which facilitates uniform Zn^{2+} deposition on the (002) crystal plane (Fig. 1b).[22]

To validate our strategy, we use a superspreading-photoinitiated method to fabricate a sodium carboxymethyl cellulose (CMC) and poly-acrylamide (PAM) polymer network *in situ* on the surface of the Zn anode. As shown in Fig. 1c, the mixed pre-polymerization solution spread rapidly and entirely (defined as superspreading) (Movie S1, Fig. S1) on the plasma-treated surface of the Zn anode.[23–26] Subsequently, UV irradiation yielded the *in situ* polymerized hydrogel electrolyte (abbreviated as SP-CMC-PAM). This strategy is also easily carried out for large-scale preparation (Fig. 1d). The FTIR results illustrate that the disappearance of the AM monomer peaks at 3340 and 3150 cm^{-1} after polymerization verifies the formation of a chemically cross-linked PAM network (Fig. S2). Furthermore, the red-shifting of the N–H peaks in the CMC-PAM hydrogel spectrum compared to pure AM and CMC indicates hydrogen bonding between the PAM and CMC polymers.[27] The scanning electron microscopy (SEM) images revealed the morphology of the SP-CMC-PAM hydrogel (Fig. S3a and b), displaying a continuous, porous network structure that facilitates rapid Zn^{2+} ion transport.[28]

The initial electric field distribution plays a key role in the Zn nucleation process, and the poor flatness of Zn surfaces typically leads to uneven electrodeposition due to an inhomogeneous electric field distribution.[29,30] Thus, we investigated the surface morphology of Zn anodes before and after plasma treatment. Notably, the surface of the Zn anode showed no significant change after plasma treatment owing to the high hardness of Zn metal (Fig. S4a and b). X-ray photoelectron spectroscopy (Fig. S5a) reveals a shift of the O 1s peak towards higher binding energies after plasma treatment, indicating the successful introduction of high oxidation state oxygen-containing functional groups (such as hydroxyl and carboxyl groups) onto the Zn surface and a consequent enhancement of its hydrophilicity. To verify the strong bonding between the hydrogel and the Zn anode, we first measured the interfacial peel strength (Fig. 1e). The SP-CMC-PAM bonded to the Zn anode exhibited a significantly higher peel strength (3.76 N m^{-1}) compared to the physically attached CMC-PAM (0.88 N m^{-1}). Then a dense interface with tight bonding between SP-CMC-PAM and the Zn anode was revealed by SEM images (Fig. 1g), whereas voids existed between CMC-PAM and the Zn anode, forming a weak bonding interface (Fig. 1f). Furthermore, high-resolution Zn 2p spectra (Fig. S5b) confirmed chemical

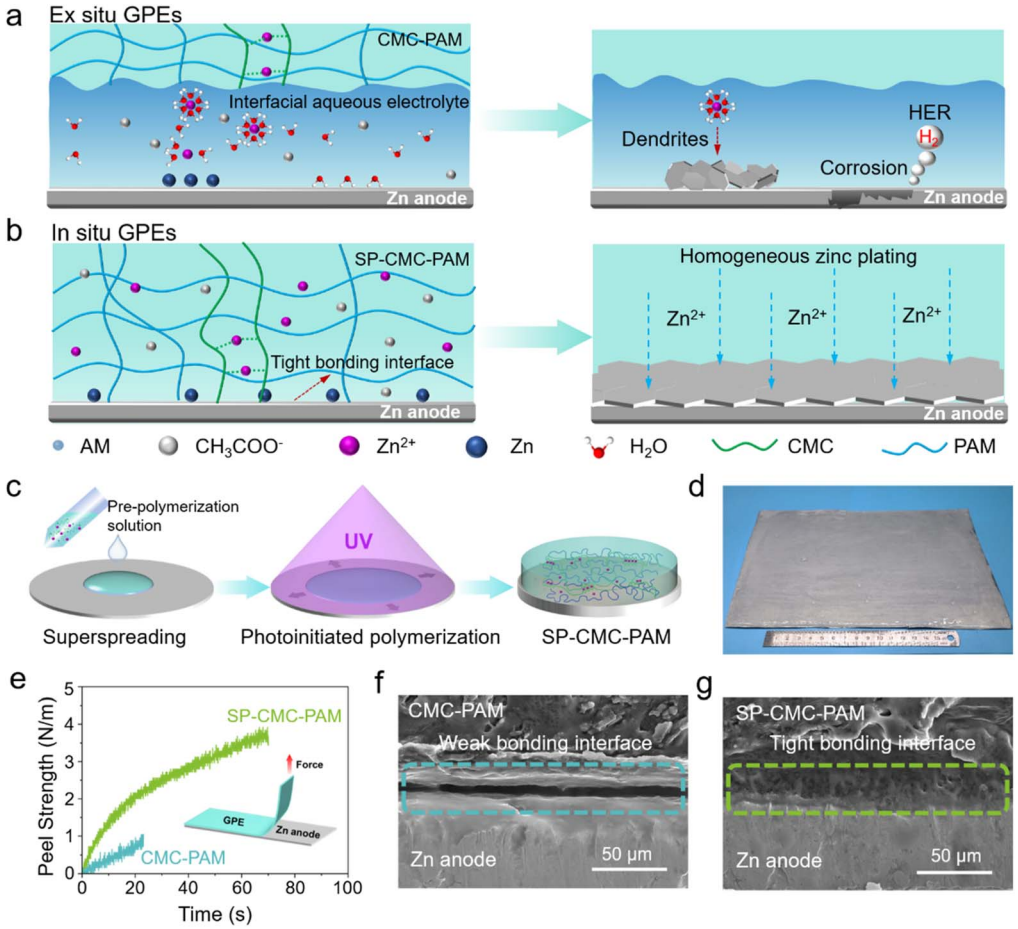

Fig. 1 (a) Schematic of *ex situ* GPEs and (b) *in situ* GPEs at the electrode–electrolyte interface. (c) Preparation of SP-CMC-PAM polymerized *in situ* on the Zn anode. (d) Photographs showing the large-area SP-CMC-PAM hydrogel electrolyte on the Zn anode. (e) 90° peel strength with the Zn anode as a substrate. (f and g) SEM images of the GPEs/Zn anode interface for CMC-PAM and SP-CMC-PAM.

interactions at the hydrogel-Zn anode interface. The presence of Zn species with lower valence states, evidenced by peaks centered at 1021 eV and 1044 eV, strongly suggests chemical bonding between Zn and functional groups within the hydrogel.[31]

SP-CMC-PAM-induced even deposition and fast ion transport

To investigate the homogeneous deposition of Zn^{2+} induced by SP-CMC-PAM, we analyzed the morphological changes of cycled Zn electrodes using Zn//Zn symmetric cells. After 100 cycles, we observed a large number of layered dendrites on the Zn surface in the CMC-PAM electrolyte (Fig. S6a). Conversely, the SP-CMC-PAM hydrogel electrolyte promoted a more homogeneous coating on the Zn surface, indicating the progressive development of a uniform deposition architecture with favorable morphology during cycling (Fig. S6b). Atomic force microscopy analysis also further confirmed that SP-CMC-PAM exhibits superior surface uniformity compared to CMC-PAM (Fig. 2a–c). In order to accurately probe the short-circuit failure mechanism of Zn anodes, we characterized Zn//Zn morphology under varying current densities. In the CMC-PAM, dendrites can be observed on the Zn surface. When the areal capacity is 1 mA h cm^{-2}, vertically aligned nanosheet-like dendrites can be seen on the Zn anode surface. At capacities of 2 mA h cm^{-2} and 4 mA h cm^{-2}, a rapid accumulation can be observed (Fig. 2d). In contrast, in the SP-CMC-PAM the surface of the Zn anodes showed smooth surfaces without dendrite formation when the areal capacities were 1 mA h cm^{-2}, 2 mA h cm^{-2}, and 4 mA h cm^{-2} (Fig. 2e). It was shown that the SP-CMC-PAM hydrogel electrolyte significantly inhibited the growth of Zn dendrites.

The crystal structure of the Zn anode surface after cycling of Zn//Zn symmetric cells containing different electrolytes was investigated by X-ray diffraction (XRD). The pristine Zn anode exhibited an intensity ratio of the $Zn_{(002)}$ surface to the $Zn_{(101)}$ surface expressed as $I_{(002)}/I_{(101)}$ of 0.59 (Fig. S7a). After cycling in the SP-CMC-PAM, $I_{(002)}/I_{(101)}$ increased significantly to 0.67, which is higher than $I_{(002)}/I_{(101)}$ (0.56) in the CMC-PAM, indicating that SP-CMC-PAM could induce preferential (002) deposition (Fig. S7b).[32,33] In contrast, after cycling in zinc acetate liquid electrolyte, $I_{(002)}/I_{(101)}$ became smaller (0.09), implying a random deposition behavior and producing a large number of zinc dendrites. The reversibility of Zn plating/stripping was assessed using Zn//Ti asymmetric cells. The cell containing SP-

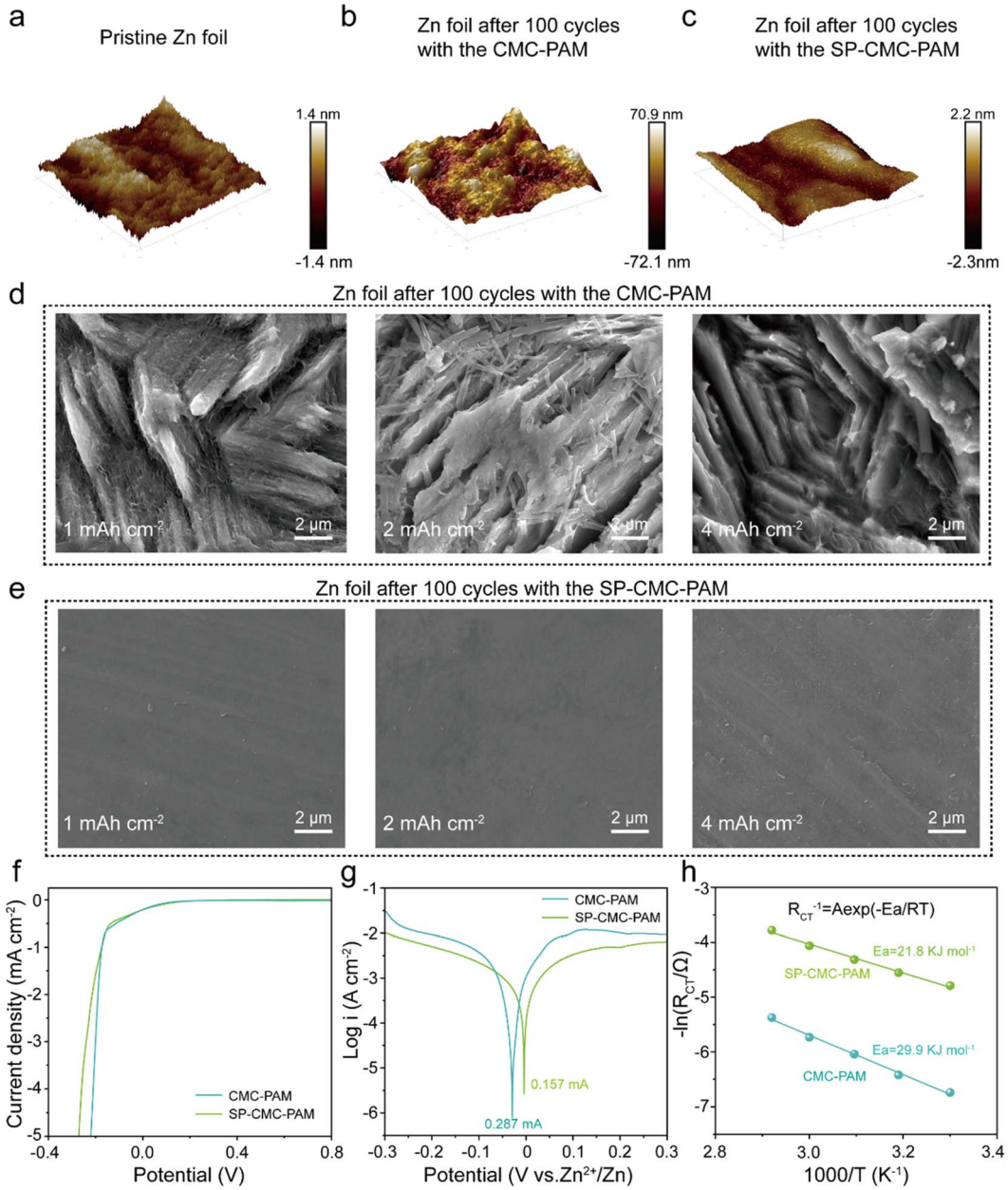

Fig. 2 The effect of CMC-PAM and SP-CMC-PAM on the corrosion and deposition behaviour of Zn anodes. AFM images of Zn anodes at (a) the pristine state and the deposited states after cycling for 100 cycles in Zn//Zn symmetric cells with (b) CMC-PAM and (c) SP-CMC-PAM electrolytes. The cross-section SEM images of the Zn anode in (d) CMC-PAM and (e) SP-CMC-PAM electrolytes after plating of 1 mA h cm^{-2}, 2 mA h cm^{-2} and 4 mA h cm^{-2}. (f) LSV curves and (g) linear polarization curves in CMC-PAM and SP-CMC-PAM electrolytes. (h) Arrhenius curves and the corresponding calculated desolvation activation energies.

CMC-PAM demonstrated a stable coulombic efficiency of 99.7% (Fig. S8), further demonstrating excellent reversibility.[34]

In order to further explore the failure mechanism of Zn plating/stripping processes, we investigated the electrochemical properties of different electrolytes. The HER was delayed in the SP-CMC-PAM hydrogel electrolyte compared to the CMC-PAM hydrogel electrolyte, indicating improved corrosion resistance (Fig. 2f). In the SP-CMC-PAM hydrogel electrolyte, the Zn anodic corrosion current calculated from the Tafel curve was 0.157 mA, which was significantly lower than the corrosion current (0.287 mA) in the CMC-PAM electrolyte (Fig. 2g). This improvement is attributed to the formation of coordination bonds at the Zn anode-hydrogel electrolyte interface and the abundance of hydrophilic groups (*e.g.*, carboxyl, hydroxyl, amide) within the dense interfacial polymer network (Fig. S9). These factors promote the conversion of more free water at the interface into bound water; in the gel close to the Zn anode, the free water content (22%) is significantly lower than that in the liquid electrolyte (44%) and the gel located away from the Zn anode (30%), as confirmed by Raman spectroscopy (Fig. S10). The

coordination bonds and enhanced hydrogen bonding interactions at the electrode–electrolyte interface contribute to locking free water, thereby reducing the electrochemical activity of free water and suppressing side reactions.[35] In addition, the synergistic effect of rapid desolvation kinetics and high Zn^{2+} migration number is critical for inhibiting zinc dendrite growth.[36] Therefore, we calculated the activation energies for hydrated Zn^{2+} desolvation using the Arrhenius equation for both the SP-CMC-PAM hydrogel electrolyte and the CMC-PAM hydrogel electrolyte (Fig. 2h, S11 and 12), which were 21.8 and 29.9 kJ mol^{-1}, respectively. This indicated that the SP-CMC-PAM hydrogel electrolyte can remove the water sheath of $[Zn(H_2O)_6]^{2+}$ and accelerate the desolvation process. Moreover, the low charge transfer resistance indicated a more efficient charge transfer process and faster plating kinetics at the Zn anode. This was attributed to the high ionic conductivity network and abundant active sites of the SP-CMC-PAM hydrogel electrolyte (Fig. S13).[37] The synergy of high ionic conductivity and elevated Zn^{2+} transference number optimizes ion transport kinetics. This facilitates efficient charging/discharging, suppresses polarization, and thereby achieves dendrite growth suppression and prolonged cycle life.[38,39]

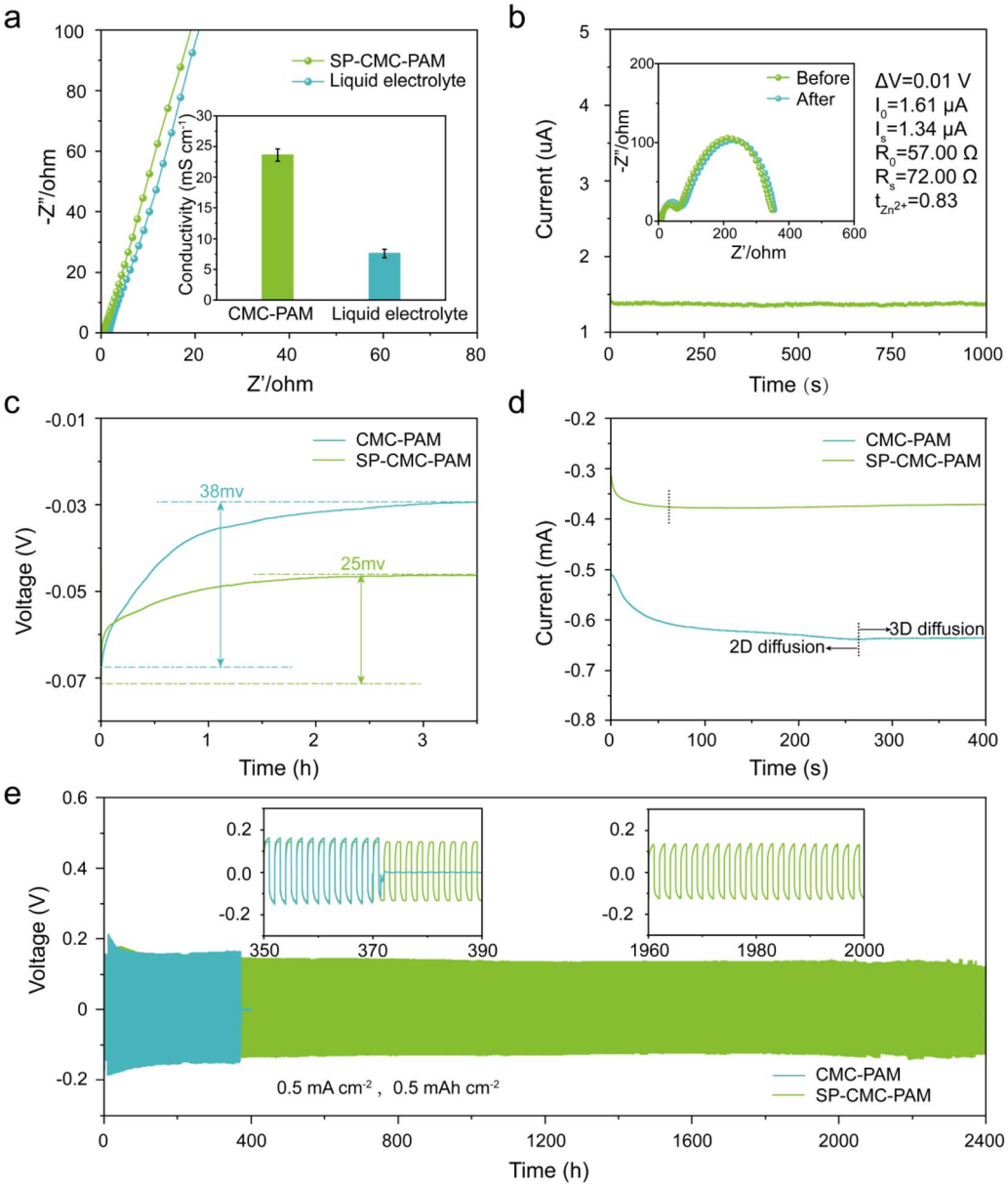

Fig. 3 (a) Nyquist plots of SP-CMC-PAM and liquid electrolytes (inset: the corresponding ionic conductivity). (b) *I–t* curve of the Zn//Zn symmetric cell (inset: Nyquist plots before and after polarization). (c) Initial nucleation curves of Zn deposition in CMC-PAM and SP-CMC-PAM, respectively, at a current of 0.1 mA cm^{-2}. (d) Chronoamperometry tests of Zn metal with CMC-PAM and SP-CMC-PAM electrolytes at an overpotential of −150 mV. (e) Voltage profiles of Zn plating/stripping for Zn//Zn symmetric cells with CMC-PAM and SP-CMC-PAM at 0.5 mA cm^{-2}/0.5 mA h cm^{-2}.

The ionic conductivity of the SP-CMC-PAM hydrogel electrolyte by electrochemical impedance spectroscopy was measured to be 23.6 mS cm^{-1}, significantly higher than that of the liquid electrolyte (9 mS cm^{-1}) (Fig. 3a). Meanwhile, the Zn^{2+} transference number ($t_{Zn^{2+}}$) was calculated by the steady-state current method to verify the fast ionic mobility of the SP-CMC-PAM system. The SP-CMC-PAM hydrogel electrolyte exhibited a higher Zn^{2+} transference number (0.83) compared to the CMC-PAM hydrogel electrolyte (0.67) (Fig. 3b and S14). These results suggest that the SP-CMC-PAM hydrogel electrolyte, leveraging its polar functional groups and additional ion transport pathways, effectively regulates Zn^{2+} deposition behavior. The uniform ion flux distribution and reduced interfacial concentration polarization thereby further mitigate the random dendrite growth.

We further investigated the performance of SP-CMC-PAM and CMC-PAM hydrogel electrolytes in Zn//Zn symmetric cells. As shown in Fig. 3c, at a current density of 0.1 mA cm^{-2}, the cell with the SP-CMC-PAM hydrogel electrolyte exhibited a lower initial nucleation overpotential (25 mV), which was much lower than that of the cell with the CMC-PAM hydrogel electrolyte (38 mV). This suggests that SP-CMC-PAM is effective in reducing the nucleation potential for Zn deposition.

To further explore the difference in deposition behavior, a chronoamperometry test was performed (Fig. 3d). This test monitored the change of current with time at a constant potential (−0.15 V), revealing the nucleation and subsequent

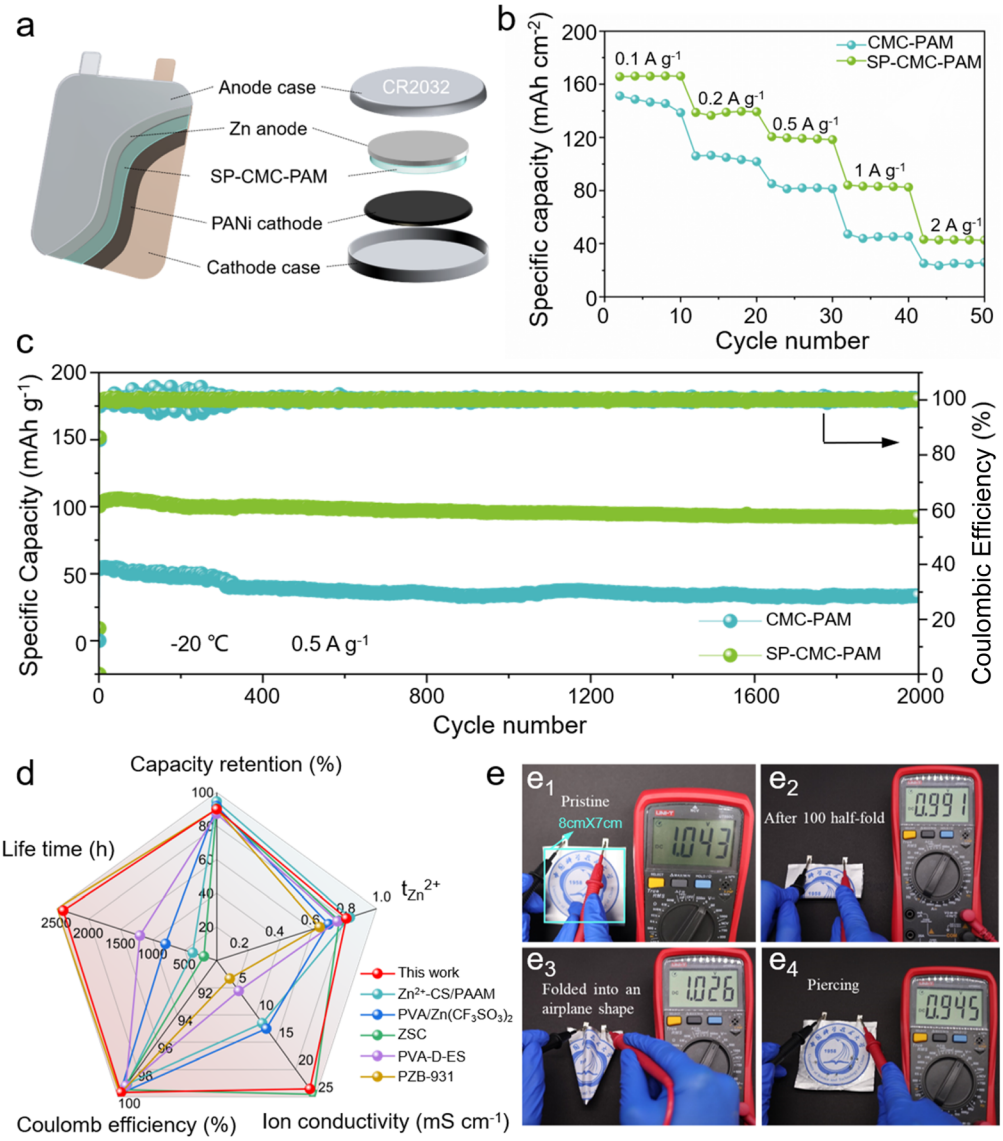

Fig. 4 Full cell test and device demonstration. (a) Schematic diagram of the structure of pouch full batteries and button full batteries, (b) rate capabilities of Zn//PANi full batteries at various current densities from 0.1 to 2 A g^{-1} at 25 °C. (c) Cycling performance of Zn/CMC-PAM/PANi and Zn/SP-CMC-PAM/PANi full batteries at 0.5 A g^{-1} and −20 °C. (d) Comparison of various electrochemical properties with reported GPEs, the details are contained in Table S1 within the SI. (e) Zn/SP-CMC-PAM/PANi pouch cell (length is 8 cm, width is 7 cm) voltages under different test conditions, including pristine state, 100 half-fold, folded into an airplane shape and piercing.

diffusion mechanism of Zn. In the CMC-PAM hydrogel electrolyte, the scarcity of active sites on the Zn anode surface led to adsorbed Zn^{2+} ions undergoing predominantly two-dimensional (2D) lateral diffusion in search of energetically favorable deposition sites. This resulted in a sustained rise in deposition current over 263 seconds. In sharp contrast, in the SP-CMC-PAM hydrogel electrolyte, the chronoamperometric profile showed stabilization of the current density within 67 seconds. This strongly suggests that the dense interfacial polymer network of the SP-CMC-PAM hydrogel electrolyte provided abundant ion channels and active sites, promoting three-dimensional (3D) diffusion of Zn^{2+}. These results confirm that *in situ* construction of hydrogel electrolytes on the Zn anode surface is essential for eliminating electrode–electrolyte interfacial impedance, thereby establishing the foundation for uniform zinc nucleation and growth.[40,41]

Electrochemical performance of symmetric/full cells in SP-CMC-PAM

In order to evaluate the stability and reversibility of Zn anodes, long-term galvanostatic cycling performances were evaluated in Zn//Zn symmetric cells. With the assistance of the SP-CMC-PAM hydrogel electrolyte, the Zn anode maintained a significantly extended lifespan of up to 2400 h at 0.5 mA cm^{-2} and 0.5 mA h cm^{-2}, which was all higher than that in the CMC-PAM hydrogel electrolyte and in the liquid electrolyte (Fig. 3e, S15 and S16). In addition, after cycling, the SP-CMC-PAM maintains a stable interface with the Zn anode, while the interface between CMC-PAM and the zinc anode deteriorates further (Fig. S17) and the Zn anode's surface in the SP-CMC-PAM system displays a smooth and dense deposition layer. In contrast, the Zn anode's surface in the CMC-PAM system exhibits irregular lamellar deposition with dendritic growth (Fig. S18).

To further demonstrate the improved electrochemical stability of SP-CMC-PAM towards the interface, we also assembled Zn/SP-CMC-PAM/PANi full cells (Fig. 4a). The Zn/SP-CMC-PAM/PANi full cells at different current densities (0.1, 0.2, 0.5, 1, and 2 A g^{-1}) exhibited excellent multiplicity performances of 166, 139, 121, 83, and 43 mA h g^{-1} (Fig. 4b), all higher than the multiplicity performance of Zn/CMC-PAM/PANi, respectively, at 25 °C. Furthermore, after 2000 cycles at 0.5 A g^{-1} current density, it still had a specific capacity of 100 mA h g^{-1} (Fig. S19).

The new generation of flexible aqueous Zn-ion batteries remains a challenge for practical applications that require improved electrochemical performance in extreme environments, especially when operating at sub-zero temperatures.[42,43] We tested Zn/PANi full cells with different electrolytes at −20 °C, and at a high current density of 0.5 A g^{-1} (Fig. 4c), the Zn/SP-CMC-PAM/PANi cell provided a reversible capacity of 100.4 mA h g^{-1}, with a much higher capacity retention rate of 91% after 2000 cycles. This is attributed to the stable electrode–electrolyte interface, the rich hydrogen-bonded polymer network, and the zinc acetate-potassium acetate electrolyte system, which collectively improve interfacial ion transport ability and provide good low-temperature resistance.[44] In the CMC-PAM, only 53.7 mA h g^{-1} of initial capacity was observed when operated at 0.5 A g^{-1}, with poor cycling stability (64.4% capacity retention after 2000 cycles), which also demonstrated the advantages of SP-CMC-PAM-induced fast ion transport at low temperature.

Through the above comparison of electrochemical performance, it is clear that the SP-CMC-PAM cells have a competitive advantage over the recently reported GPE cells in terms of capacity retention, cycle life, coulombic efficiency, ion conductivity and Zn^{2+} transference number as shown in Fig. 4d and Table S1.[45–49] In addition, we assembled a pouch full battery (length is 8 cm, width is 7 cm) to validate the practical application of the SP-CMC-PAM hydrogel electrolyte (Fig. 4e). Fig. $4e_1$ shows the pristine voltage of the pouch cell. The pouch battery exhibited stable initial voltage and only minor voltage fluctuations after being folded in half 100 times (Fig. $4e_2$). We also folded the pouch battery into an airplane shape, and the voltage readings showed no significant changes (Fig. $4e_3$). Even when the pouch battery was pierced, there were only minor voltage fluctuations (Fig. $4e_4$). Through these destructive tests, the SP-CMC-PAM pouch battery demonstrated excellent stability and resistance to damage, attributed to the tight bonding at the electrode–electrolyte interface and good flexibility. These characteristics will facilitate the potential application of the SP-CMC-PAM hydrogel electrolyte in flexible batteries.

Conclusion

In summary, we report a strategy for constructing an SP-CMC-PAM hydrogel *in situ* on a Zn anode. This approach leverages the pre-polymerization solution's superspreading properties on the superhydrophilic surface combined with *in situ* photo-initiated polymerization. The resulting hydrogel electrolyte forms a strongly adhered, integrated interface with the anode, which effectively inhibits Zn dendrite growth and side reactions. Consequently, the assembled battery exhibits significantly enhanced cycling stability and rate capability. This work provides an effective way to solve the challenge of Zn anode-electrolyte interface stability in commercial AZIBs, and paves a new way to achieve high-performance and high-safety zinc-ion batteries.

Author contributions

Chuangqi Zhao supervised this project and conceived and designed this work. Jihao Fan conducted the investigation, experiments, and data analysis, and wrote the manuscript. Ziqiang Zhao and Shengwen Kong performed the data analysis and contributed to software development. Jihao Fan and Linlin Ma reviewed and commented on this work and performed the validation. Chuangqi Zhao, Linlin Ma, Shengwen Kong and Yanglansen Cui discussed the results, and revised and edited this manuscript. Chuangqi Zhao and Yanglansen Cui conducted the morphological analysis. All authors discussed the final manuscript.

Conflicts of interest

The authors declare no conflicts of interest.

Data availability

The data that support the findings of this study are available from the corresponding author upon reasonable request.

Supplementary information (SI) is available. See DOI: https://doi.org/10.1039/d6ta00298f.

Acknowledgements

This research was supported by the National Natural Science Foundation of China (22305244, 2252200918 and 22405267); The Start-up Funding for Suzhou Institute for Advanced Research, University of Science and Technology of China (KY2260080033); The Start-up Funding for University of Science and Technology of China (KY2060000233); CAS Hundred Talent Program (KJ2060007007); and Suzhou Key Laboratory of Bio-inspired Interfacial Science (SZ2024004). The authors thank the Physical and Chemical Analysis Center at Suzhou Institute for Advanced Research, University of Science and Technology of China.

References

1 S. W. D. Gourley, R. Brown, B. D. Adams and D. Higgins, *Joule*, 2023, **7**, 1415–1436.
2 Y. Liang and Y. Yao, *Nat. Rev. Mater.*, 2023, **8**, 109–122.
3 N. Zhang, X. Chen, M. Yu, Z. Niu, F. Cheng and J. Chen, *Chem. Soc. Rev.*, 2020, **49**, 4203–4219.
4 Z. Yi, G. Chen, F. Hou, L. Wang and J. Liang, *Adv. Energy Mater.*, 2021, **11**, 2003065.
5 Y. Zhu, G. Liang, X. Cui, X. Liu, H. Zhong, C. Zhi and Y. Yang, *Energy Environ. Sci.*, 2023, **17**, 369–385.
6 Z. Cheng, J. Fu, P. Kang, H. Yao, F. Mo and H. Hu, *Adv. Energy Mater.*, 2025, **15**, 2405767.
7 Y. Wang, Q. Li, H. Hong, S. Yang, R. Zhang, X. Wang, X. Jin, B. Xiong, S. Bai and C. Zhi, *Nat. Commun.*, 2023, **14**, 3890.
8 B. Zhang, L. Qin, Y. Fang, Y. Chai, X. Xie, B. Lu, S. Liang and J. Zhou, *Sci. Bull.*, 2022, **67**, 955–962.
9 Q. Deng, W. Zhou, H. Wang, Q. Ma, C. Li, X. Wu and Y. Wu, *Energy Mater.*, 2025, **5**, 500103.
10 Y. Zhou, Y. Zhang, Y. Nie, D. Sun, D. Wu, L. Ban, H. Zhang, S. Yang, J. Chen, H. Du and X. Pan, *Prog. Mater. Sci.*, 2025, **152**, 101460.
11 X. Li, Y. Li, R. Wang, D. Wang and F. Ran, *Chem. Eng. J.*, 2024, **496**, 153865.
12 L. Xu, T. Meng, X. Zheng, T. Li, A. H. Brozena, Y. Mao, Q. Zhang, B. C. Clifford, J. Rao and L. Hu, *Adv. Funct. Mater.*, 2023, **33**, 2302098.
13 S. Cui, X. Wang, W. Miao, X. Wang, X. Li, M. Xun, K. Sun, H. Peng and G. Ma, *Energy Storage Mater.*, 2024, **68**, 103356.
14 G. Dai, Y. Zhou, Z. Liu, J. Liu, K. Tan, L. Xu, Y. Chen, J. Du and A. Sun, *Chem. Eng. J.*, 2025, **525**, 170644.
15 J. Liu, Q. Dang, J. Yuwono, S. Zhang, Z. Tai, Z. Guo and Y. Liu, *Nano-Micro Lett.*, 2025, **17**, 292.
16 Y. Hao, D. Feng, L. Hou, T. Li, Y. Jiao and P. Wu, *Adv. Sci.*, 2022, **9**, 2104832.
17 X. Lei, X. Liu, W. Ma, Z. Cao, Y. Wang and Y. Ding, *Angew. Chem., Int. Ed.*, 2018, **57**, 16131–16135.
18 Y. Qin, H. Li, C. Han, F. Mo and X. Wang, *Adv. Mater.*, 2022, **34**, 2207118.
19 Y. G. Cho, C. Hwang, D. S. Cheong, Y. S. Kim and H. K. Song, *Adv. Mater.*, 2019, **31**, 1804909.
20 Y. Cui, W. Chen, W. Xin, H. Ling, Y. Hu, Z. Zhang, X. He, Y. Zhao, X. Kong, L. Wen and L. Jiang, *Adv. Mater.*, 2024, **36**, e2308639.
21 L. Ma, Q. Li, Y. Ying, F. Ma, S. Chen, Y. Li, H. Huang and C. Zhi, *Adv. Mater.*, 2021, **33**, e2007406.
22 C. Li, J. Wang, D. Zhang, M. Li, H. Chen, W. Yi, X. Ren, B. Liu, X. Lu and M. Liu, *J. Energy Chem.*, 2024, **97**, 342–351.
23 L. Ma, X. Liu, J. Fan, X. Yu, L. Cao and C. Zhao, *Mater. Horiz.*, 2025, **12**, 2736–2744.
24 S. Kong, C. Zhao, Y. Sun, J. Huang, L. Zhang, Y. Ru, H. Zhou, T. Zhou and M. Liu, *Matter*, 2024, **7**, 2250–2264.
25 X. Liu, L. Ma, C. Zhou, L. Liu, C. Qian, C. Zhao and L. Jiang, *Interdiscip. Mater.*, 2025, **4**, 333–342.
26 C. Zhao, P. Zhang, J. Zhou, S. Qi, Y. Yamauchi, R. Shi, R. Fang, Y. Ishida, S. Wang, A. P. Tomsia and M. Liu, *Nature*, 2025, **580**, 210–215.
27 J. Bai, R. Wang, X. Wang, S. Liu, X. Wang, J. Ma, Z. Qin and T. Jiao, *Cell Rep. Phys. Sci.*, 2021, **2**, 100623.
28 B. Villagra Di Carlo and A. C. Habert, *J. Mater. Sci.*, 2013, **48**, 1457–1464.
29 H. Jia, M. Qiu, C. Lan, H. Liu, M. Dirican, S. Fu and X. Zhang, *Adv. Sci.*, 2022, **9**, e2103952.
30 X. Wu, Y. Chen, B. Tang, Q. Yan, D. Wu, H. Zhou, H. Wang, H. Zhang, D. He, H. Li, J. Zeng, L. Lu, S. Yang and T. Ma, *Nat. Commun.*, 2025, **16**, 8785.
31 C. Tian, J. Wang, R. Sun, T. Ali, H. Wang, B. Xie, Y. Zhong and Y. Hu, *Angew. Chem., Int. Ed.*, 2023, **62**, e202310970.
32 L. Xu, T. Meng, X. Zheng, T. Li, A. H. Brozena, Y. Mao, Q. Zhang, B. C. Clifford, J. Rao and L. Hu, *Adv. Funct. Mater.*, 2023, **33**, 2302098.
33 Z. Wang, J. Diao, J. N. Burrow, K. K. Reimund, N. Katyal, G. Henkelman and C. B. Mullins, *Adv. Funct. Mater.*, 2023, **33**, 2304791.
34 Z. Wu, Y. Wang and C. Zhi, *Joule*, 2024, **8**, 2442–2448.
35 Q. Zhang, Y. Zhang, L. Ke, H. Jiang, Y. Huang, Z. Nie and S. Jin, *J. Mater. Sci. Technol.*, 2024, **225**, 40–48.
36 B. Song, Q. Lu, X. Wang and P. Xiong, *Energy Mater.*, 2025, **5**, 500031.
37 H. Lu, J. Hu, L. Wang, J. Li, X. Ma, Z. Zhu, H. Li, Y. Zhao, Y. Li, J. Zhao and B. Xu, *Adv. Funct. Mater.*, 2022, **32**, 2112540.
38 Z. Shi, M. Yang, Y. Ren, Y. Wang, J. Guo, J. Yin, F. Lai, W. Zhang, S. Chen, H. N. Alshareef and T. Liu, *ACS Nano*, 2023, **17**, 21893–21904.
39 M. Zhou, S. Guo, J. Li, X. Luo, Z. Liu, T. Zhang, X. Cao, M. Long, B. Lu, A. Pan, G. Fang, J. Zhou and S. Liang, *Adv. Mater.*, 2023, **33**, e2100187.

40 M. Jiao, L. Dai, H. Ren, M. Zhang, X. Xiao, B. Wang, J. Yang, B. Liu, G. Zhou and H. Cheng, *Angew. Chem., Int. Ed.*, 2023, **135**, e202301114.
41 D. Wu, H. Wang, Y. Nie, H. Wan, S. Liu, S. Yang, H. Li, H. Zhang, C. Zhu and T. Ma, *Prog. Mater. Sci.*, 2026, **155**, 101538.
42 Q. Zhang, Y. Ma, Y. Lu, L. Li, F. Wan, K. Zhang and J. Chen, *Nat. Commun.*, 2020, **11**, 4463.
43 Y. Yan, S. Duan, B. Liu, S. Wu, Y. Alsaid, B. Yao, S. Nandi, Y. Du, T. Wang, Y. Li and X. He, *Adv. Mater.*, 2023, **35**, 2211673.
44 S. Huang, L. Hou, T. Li, Y. Jiao and P. Wu, *Adv. Mater.*, 2022, **34**, 2110140.
45 Y. Liu, A. Gao, J. Hao, X. Li, J. Ling, F. Yi, Q. Li and D. Shu, *Chem. Eng. J.*, 2023, **452**, 139605.
46 S. Huang, F. Wan, S. Bi, J. Zhu, Z. Niu and J. Chen, *Angew. Chem., Int. Ed.*, 2019, **58**, 4313.
47 F. Mo, Z. Chen, G. Liang, D. Wang, Y. Zhao, H. Li, B. Dong and C. Zhi, *Adv. Energy Mater.*, 2020, **10**, 2000035.
48 J. Kang, Z. Jiang and L. Wen, *Adv. Funct. Mater.*, 2025, 2422566.
49 M. Wang, A. Emre, S. Tung, A. Gerber, D. Wang, Y. Huang, V. Cecen and N. A. Kotov, *ACS Nano*, 2019, **13**, 1.